Environ Earth Sci (2016) 75:212
DOI 10.1007/s12665-015-4770-3

ORIGINAL ARTICLE

Salt bursting tests on volcanic tuff rocks from Mexico

R. López-Doncel[1] · W. Wedekind[2] · T. Leiser[2] · S. Molina-Maldonado[4] · A. Velasco-Sánchez[4] · R. Dohrmann[3] · A. Kral[2] · A. Wittenborn[2] · A. Aguillón-Robles[1] · S. Siegesmund[2]

Received: 26 March 2015 / Accepted: 21 July 2015 / Published online: 25 January 2016

Abstract During the pre-colonial period all the architectural constructions of the Maya and the later Aztec culture were made from different types of rocks available in the nearby surroundings of the settlements. Later, the architecture characterizing the Spanish colonization utilized volcanic tuff rocks for ashlars and masonry facades. Volcanic tuffs were used in large quantities and are still the main natural building rock used in most of the country. Tuffs are mostly soft and porous rocks that can be easily cut and reworked. They are, however, very susceptible to the effects of weathering, especially the deterioration caused by salt crystallization. Seventeen volcanic tuff samples from Mexico used as natural building stones were studied. These tuffs show highly variable compositions and different porosities and textural properties as well as very different behaviors in regard to salt crystallization. The petrographic, petrophysical, mineralogical and geochemical properties of the 17 samples were analyzed before and after a large number of salt bursting tests in order to try and determine the main factors leading to the weathering caused by salt crystallization. Some factors appear to have a real importance in regard to the resistance against salt crystallization. Two of the most important are the water vapor diffusion (μ value) and the pore radii distribution; however, microporosity also becomes a relevant factor for rapid salt destruction if it reaches more than 50 % of the pore volume. All these effects related to the salt crystallization are dependent on the presence of water in any form, so the climatic conditions must also play a principal role.

Keywords Salt bursting · Volcanic tuff rocks · Pore radii distribution · Mexico

✉ R. López-Doncel
rlopez@uaslp.mx

[1] Instituto de Geología, Universidad Autónoma de San Luis Potosí, San Luis Potosí, Mexico

[2] Geowissenschaftliches Zentrum der Universität Göttingen, Göttingen, Germany

[3] Bundesanstalt für Geowissenschaften und Rohstoffe, Hannover, Germany

[4] Posgrado en Geología Aplicada, Universidad Autónoma de San Luis Potosí, San Luis Potosí, Mexico

Introduction

All the pre-colonial constructions of the Maya and later Aztec culture were made from different rock types available locally, near the settlements that used a colored plaster covering (Wedekind et al. 2011), whereas during the period of Spanish colonization the architecture is characterized by ashlars and masonry facades. The available rocks were transported within a geographic radius of about 100 km. After the second half of the sixteenth century many important cities were built whose main buildings were constructed almost exclusively with natural rocks. Due to the abundance of volcanic rocks throughout the country and because of the properties that vulcanites exhibit as a construction material (Wedekind et al. 2013), volcanic tuffs were mainly used in large quantities in the past and are still the main the choice for use in most of the country today. Tuffs are mostly soft and porous rocks that can be easily cut and reworked. However, they can be very susceptible to the effects of weathering, especially the deterioration caused by salt crystallization. Despite this, the effects of material loss and deterioration are visible in many different forms and levels in the analyzed tuffs in this study.

Plate 1 Different aspects of deterioration caused by salt bursting. **a**, **b** Lost material in the SG black and RG red of San Miguel de Allende. **c** Flaking in the ESC Tuff of Querétaro. **d** Sanding off in the LS Tuff of Guanajuato. **e** Back-weathering in the ZAC quarry tuff of Zacatecas and **f** salt crystallization in ESC of Querétaro

The most common types of deterioration caused by salt bursting are weathering forms like lost material (Plate 1a, b), flaking (Plate 1c), sanding off (Plate 1d), and back-weathering (Plate 1e). However, the deterioration level varies enormously from one tuff type to another, even tuffs used in modern constructions (Plate 1e) show greater damages than tuffs used in buildings older than 200 years (Plate 1d, e).

Crystallization of salts within the pores of natural building stones generate sufficient stress to provoke the cracking of stone, even up to the total destruction of the rock (Winkler and Singer 1972; Grossi and Esbert 1994; Rodriguez-Navarro and Doehne 1999; Flatt 2002; Tsui et al. 2003; Coussy 2006). This process is considered to be the most important cause of deterioration in natural building rocks and monuments built by ashlars. The resistance of stone to salt

Table 1 Seventeen analyzed volcanic tuffs, their color, composition and abbreviation

Sample name	Abbreviation	Classification	Provenance	30 % weight reduction by salt bursting test cycles
Red Tuff	RG	Andesite Tuff	San Miguel de Allende, Guanajuato	8
Gris Oscura Tuff	SG	Andesite Tuff	San Miguel de Allende, Guanajuato	8
Black Tuff	Qro black	Trachyte andesite Tuff	Queretaro City	10
Zacatecas Quarry	Zac quarry	Rhyolite Ignimbrite Tuff	Guadalupe, Zacatecas	11
Toba Negra	GF black	Trachyte Tuff	San Miguel de Allende, Guanajuato	12
Toba Gris	GF gray	Trachyte Tuff	San Miguel de Allende, Guanajuato	13
Zacatecas Cathedral Tuff	Zac Cath	Rhyolite ignimbrite Tuff	Zacatecas City	13
El Salto Tuff	Zac El Salto	Rhyolite glass Tuff	Zacatecas City	15
Gris de Remedios	GR	Andesite lapilli Tuff	Mexico City	16
Bufa Tuff	BT	Rhyolite Tuff	Guanajuato City	22
Blanca de Pachuca	BP	Rhyolite-Tuff	Pachuca, Hidalgo	23
Losero Formation	LS	Epiclastic Tuff	Guanajuato, Mexico	26
Cantera Amarilla Tuff	CA GDL	Rhyolite Tuff	Guadalajara, Mexico	28
Tenayocátelt Tuff	TY	Rhyolite Ignimbrite Tuff	Mexico City	38
Las Escolásticas Tuff	ESC	Rhyolite Tuff	Las Escolásticas, Querétaro	44
Cantera Rosa Tuff	CR	Rhyolite Tuff	San Miguel el Alto, Jalisco	53
Chiluca	CH	Pyroxene andesite Tuff	Mexico City	59

damage depends on the pore size distribution and decreases as the proportion of fine pores increases, therefore it is to be expected, that building rocks with a major proportion of micropores and capillary pores are less resistant against the phenomena of salt crystallization.

Fitzner and Snethlage (1982) suggest that the crystallization occurs first in the macro and capillary pores (compare with Angeli et al. 2007). The crystallization in the micropores happens when the larger pores are filled and the salt crystallization in the micropores occurs only when the chemical potential of the crystals is the same for the larger pores as for the smaller ones. Normally the crystals in the larger pores have a smaller chemical potential. This can be intensified by increasing the pressure due to crystal growth and through this process crystallization can also occur in the smaller pores. This can cause that the grain and matrix consolidation does not withstand the pressure, whereby the salt blasting begins (see also Angeli et al. 2007).

If the salt crystallization and therefore the salt bursting depend so extremely on the porosity, rocks with more and bigger pores may be more susceptible against salt blasting. Finally, all these effects related to salt crystallization are dependent on the presence of water in any form, and thus climatic conditions must also play a major role. The main goal of this work is to investigate which property of the volcanic tuff rocks plays the most important role.

To determine the main factor of the weathering caused by salt crystallization, a large number of salt bursting tests were performed on selected rock samples, which are characterized by an ideal porosity, permeability and water diffusion.

Methods

In the present study, 17 Mexican volcanic tuffs used as natural building stones were petrographically analyzed in detail (Table 1; Plates 2, 3, 4). These tuffs show varying compositions, different porosities and textural properties as well as very different behaviors in regard to salt crystallization. Tuffs are in most cases very porous rocks (up to more than 40 %, Wedekind et al. 2011, 2013; Siegesmund and Duerrast 2011) and their pore radius can vary greatly. Another characteristic of the tuff stones regarding porosity is that even if it represents a large percentage of pores in the whole rock does not necessarily mean that it is effective.

The effective porosity and the matrix- and bulk density were measured using hydrostatic weighting (DIN 52 102) on cubic stone samples (65 mm). To calculate the porosity the water-saturated mass was used, the buoyancy mass of the samples measured after water saturation under vacuum and the dry sample mass.

The moisture expansion by hydric wetting of the volcanic tuffs was determined using cylindrical samples (15 mm × 100 mm). To evaluate hydric moisture expansion, the stone cylinders were measured under water-saturated conditions (the samples were completely immersed in distilled water). The resolution of the displacement transducer is 0.1 lm and the accuracy is about 0.5 lm. The measurements were carried out on all samples parallel to the *X*, *Y*, and *Z* axes.

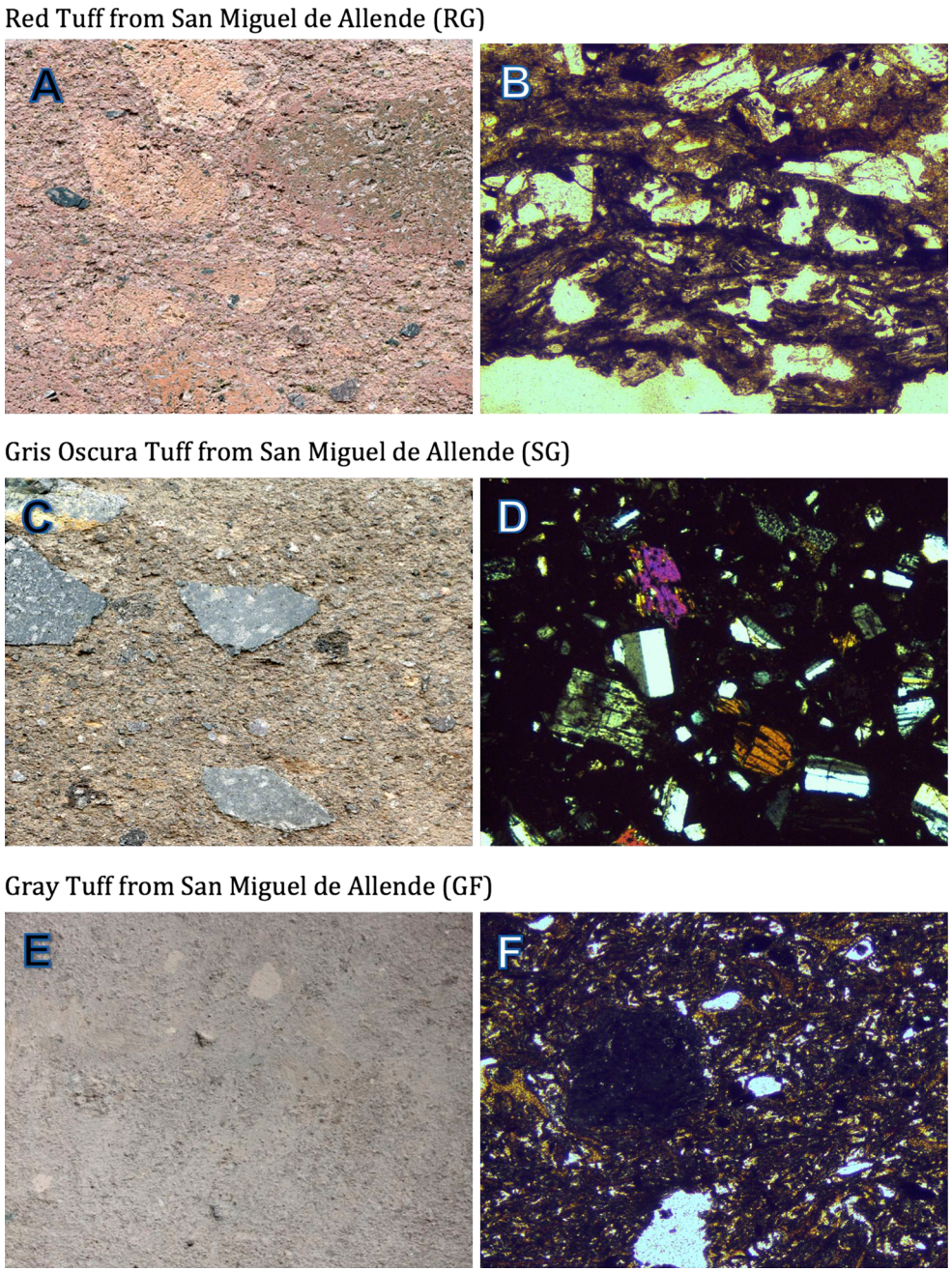

Plate 2 Tuff rocks from San Miguel de Allende. **a**, **c** and **e** macroscopic fabric in hand specimen (all samples are a 6.5 cm in length). **b**, **d** and **f** thin section of the tuff rocks from San Miguel de Allende (all microphotographs are 5 mm in length and taken with a ×5 objective), **b** and **f** parallel nicols, **d** crossed nicols

Pore size distribution was measured using the mercury intrusion porosimeter (MIP). The pore space was investigated by mercury pore size distribution as well as by thin-section analysis and SEM photographs. The water transport properties closely related to the properties of the pore space were measured by the water uptake rate and the water vapor resistance.

The capillary water absorption or water uptake was measured on cubes (65 mm) with respect to the *X*, *Y* and *Z* directions. The lower plane of the cubes was placed into water to measure the weight increase over time.

The water vapor diffusion gives information about the network of the pore system, the drying behavior and the transport mechanism controlled by the pore size distribution (Ruedrich and Siegesmund 2006). Samples of the different tuff stones were prepared in the *X*, *Y*, and *Z* directions with a diameter of 4 mm and a thickness of 10 mm and were attached to the top of Teflon cups filled with

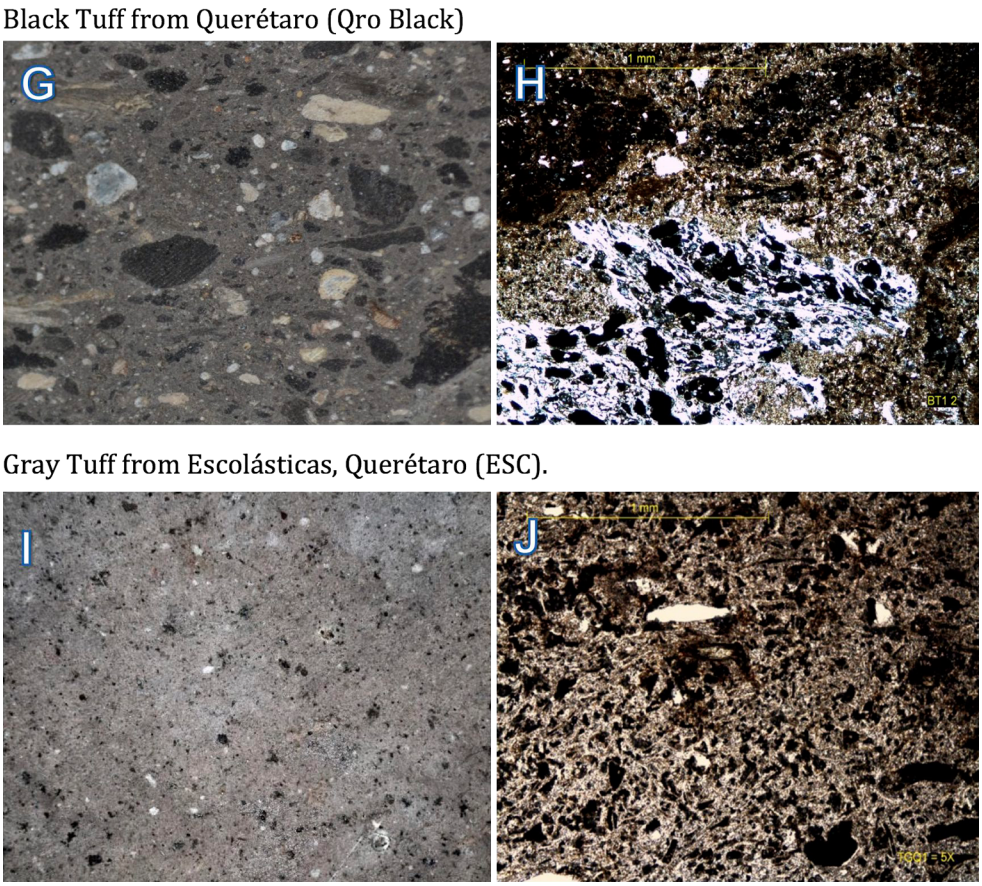

Plate 3 Tuff rocks from Querétaro. **g**, **i** Macroscopic fabric in hand specimen (all samples are a 6.5 cm in length). **h**, **j** Thin section of the tuff rocks from Querétaro (all microphotographs are 5 mm in length and taken with a ×5 objective), **h**, **j** parallel nicols

water (100 % relative humidity, RH). These cups were placed into a climate chamber at 50 % RH with a temperature of 20 °C. The weight losses of the cups were measured every 24 h. The moisture flow through the stones was calculated.

To determine the splitting tensile strength (STS) the "Brazilian test" was used, which involves disc-shaped samples 40 mm in diameter and 20 mm in length. In order to calculate the average value, a minimum of six samples was used. The splitting tensile strength was measured perpendicular to the *XY* and *XZ* planes. Tensile strength tests (STS) were conducted under dry and water-saturated conditions.

To assess the salt weathering sensitivity of the investigated tuffs in this study, a salt-weathering test according to the standard DIN EN 12370 was performed. The salt bursting test was used to investigate the resistance of the rock types to salt stress. The samples were cut into cubes (6.5 × 6.5 cm) and were soaked in a 10 % Na_2SO_4 solution. The samples spent about 4 h in the salt solution and then they were dried in an oven at 60 °C for 48 h. This process can be repeated as often as the sample allows. After each cycle, the cubes are weighed to determine the loss of material. The individual weathering progress was documented by photos.

For the analysis of the microfabrics a scanning electron microscope (SEM) ESEM FEI Quanta 600 FEG was used. The SEM was operated in the low-vacuum mode (0.6 mbar). Therefore, gold- or carbon-coated samples are not required. The microscope is equipped with an Apollo XL (AMETEK) EDX detector for microchemical analysis. The SEM sample is obtained by gently breaking the rock fragment with a small cutter. Sample preparation must be done in a clean way in order to prevent cutting shards or other materials from contaminating the sample under analysis. Optimal size for the final sample is generally around 5 mm × 10 mm × 10 mm.

Petrography

All the analyzed volcanic tuffs are Cenozoic in age and range from the Oligocene to the Holocene. Their compositions vary from acid rhyolites to basic andesite basalt.

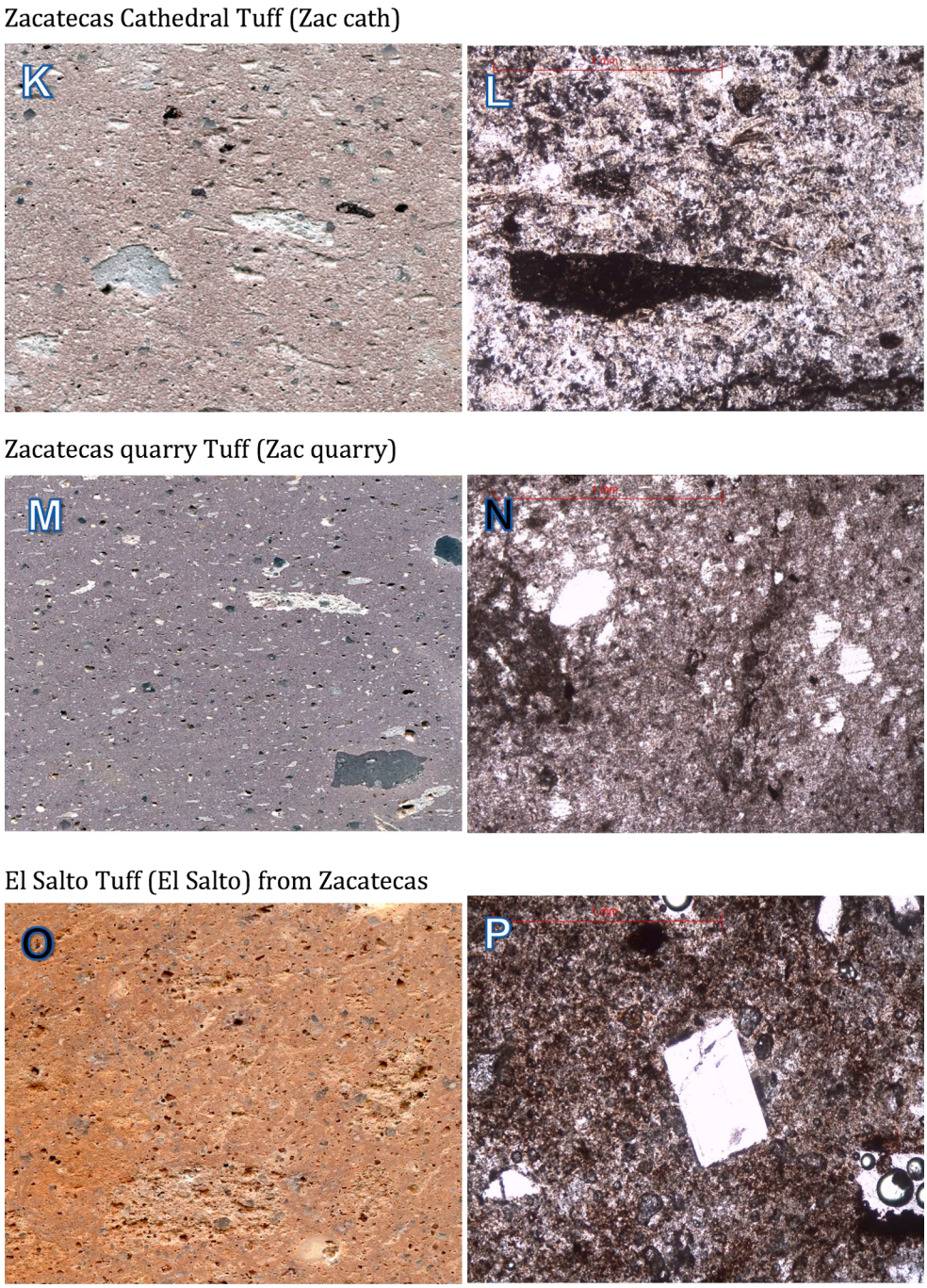

Plate 4 Tuff rocks from Zacatecas. **k**, **m** and **o**, Macroscopic fabric in hand specimen (all samples are a 6.5 cm in length). **l**, **n** and **p** Thin section of the tuff rocks from Zacatecas (all microphotographs are 5 mm in length and taken with a ×5 objective and parallel nicols)

The petrographic analysis was carried out using a polarizing microscope. Petrographic descriptions are given below.

Wedekind et al. (2011) and (2013) present a very complete petrographical description of the Blanca de Pachuca (BP), Tenayocátetl (TY), Bufa (BT), Cantera Amarilla (CA), Cantera Formation (CF), Loseros (LS), Chiluca (CH) and Cantera Rosa (CR) tuffs. This study describes the following rocks: Red Tuff (RG), Negra (SG), Gris Oscura (GF black) and Gris (GF gray) tuffs of San Miguel de Allende, the Negra (Qro black) and Escolástica (ESC) tuffs from Querétaro and the Cathedral (ZAC Cath) and El Salto (Zac El Salto) tuffs from Zacatecas (see Table 1).

Red Tuff of San Miguel de Allende (RG)

In thin section the RG shows a dark reddish, relatively coarse matrix with yellowish, whitish, grayish and orange unoriented and non-altered clasts in different sizes and textures (Plate 2a). The main mineral is plagioclase, recognized by its typical interference color, twinning and zoning. Idiomorphic olivine und fine-grained quartz crystals are also embedded in the matrix. The texture of this tuff is cryptocrystalline to glassy and a smooth flow-texture can be also observed (Plate 2b). The percentage of matrix and clasts is about 60, 40 %, respectively.

Gris Oscura Tuff of San Miguel de Allende (SG)

The Gris Oscura Tuff from San Miguel de Allende stands out because of its cm-sized, slightly oriented black clasts, which are well differentiated in the brownish–grayish matrix (Plate 2c). The matrix, comprising 70 % of the tuff, is slightly opaque under the polarizing microscope (Plate 2d). Within the matrix are also fine-grained 0.2–0.5 mm sized, well sorted, round to tabular minerals, which can be directly observed in hand specimen. The minerals are well-zoned and twinned plagioclases, brownish to reddish pyroxenes and partially altered olivines. The crystals are distributed across the whole matrix, without any orientation forming a typical seriate texture (Plate 2d), in which grains have practically the same sizes.

Black and gray Tuff of San Miguel de Allende (GF black, GF gray)

This tuff shows a very fine gray to black matrix (70 % of the rock), where 0.1 to 1 cm sized idiomorphic crystals are embedded (Plate 2e). Under the microscope the matrix shows an opaque but well-foliated texture. The opaque aspect of the matrix indicates that it is mostly made up of glass. As in the RG sample the dominant mineral are plagioclases and are the coarsest crystals. In addition to the plagioclases, some fine-grained, well-rounded, yellowish to brown mineral recognized as pyroxene occurs. Distributed within the matrix are many small opaque crystals that are probably hematite or some other iron oxides. In general the tuff shows a eutaxitic texture (Plate 2f). The main difference between the GF1 and GF2 samples is that the GF1 shows a very dark matrix, whereas the GF2 matrix is gray. Petrographically both tuffs are very similar, but the content of iron oxides in the matrix of GF1 is much larger than in the GF2.

Black Tuff of Querétaro (Qro black)

This material is a black to grayish colored pyroclastic igneous rock with a porphyritic to serial texture made up of slightly oriented non-collapsed black pumice fragments, white pumice fragments, lithics and phenocrysts of sanidine, quartz and plagioclase. The matrix has a glassy texture. The relationship between components and matrix is 65–35 %.

The black pumice comprises about 20 % of the rock and shows a highly vesicular texture (Plate 3g). These components can vary in length from 1 mm up to 30 mm and are not collapsed. The white pumice fragments make up to 20 % of the sample, are highly vesicular and also not collapsed (Plate 3g). The lithics represent about 10 % of the sample, are not very rounded and have angular to subangular broken edges and their size varies from 0.5 to 15 mm. The matrix has a glassy, non-welded ash flow tuff texture (Plate 3h) and represents 35 % of the sample.

Escolásticas Tuff of Querétaro (ESC)

This tuff is a pink to reddish, brownish colored pyroclastic igneous rock (Plate 3i) with a porphyritic texture. It is composed of unoriented lithic fragments, fiammes, non-collapsed pumice, quartz and sanidine phenocrysts hosted on a microcrystalline, devitrified reddish matrix with a eutaxitic texture. The material contains about 40 % of components and 60 % matrix.

The tuff contains about 10 % of sub to euhedral quartz with sharp angular broken edges and fractures and measures less than 1 mm in size. It also contains about 10 % of sub to euhedral sanidine crystals that have broken angular edges and have a fine grain size, less than 1 mm. The matrix is microcrystalline, devitrified well-welded mass with a eutaxitic texture and comprises up to 60 % of the sample (Plate 3j).

Cathedral Tuff of Zacatecas (Zac cath)

The sample from the cathedral of Zacatecas is a pinkish tuff with a matrix that represents 30 % of the rock. The sample exhibits a fine-grained matrix and due to iron oxides shows a pinkish coloration (Plate 4k). Under the microscope quartz phenocrysts (around 30 %) together with feldspars (10 %) and some oxides (30 %) are recognizable. Quartz phenocrysts are anhedral and supported by the matrix. Collapsed pumice clasts up to 1–10 mm in size are also embedded in the glassy, slightly foliated matrix (Plate 4l).

Quarry Tuff of Zacatecas (Zac quarry)

The sample obtained from a quarry near the city of Zacatecas consists of a pinkish–reddish tuff containing 1 cm sized well-oriented lithic clasts (Plate 4m). In thin section phenocrysts of quartz (35 %), feldspars (20 %) and

oxides (5 %) are observable. The matrix represents 40 % of the rock. The matrix is fine-grained, glassy and shows a high content of hematite (Plate 4n). The phenocrysts of quartz are anhedral and show sizes ranging up to 0.8 mm, whereas the feldspar phenocrysts are anhedral, exhibit finer grain sizes and are also distributed throughout the entire rock. The pink to red coloration is due to the oxides present in the rock.

El Salto Tuff of Zacatecas (Zac El Salto)

The sample from El Salto is a reddish–orange volcanic tuff with locally purple to dark brownish stripes and spots that gives this rock a very jazzy appearance (Plate 4o). It contains crystals of quartz (40 %), plagioclase (10 %) and some oxides (10 %). The quartz crystals are mostly anhedral and normally less than 1 mm in size. The plagioclases crystals vary from anhedral to euhedral with sizes ranging from 0.3 mm up to 1 cm (Plate 4p). The matrix, 40 % of the whole rock shows no orientation or lamination and contains an important amount in opaque crystals (oxides).

Experimental investigation and results

Petrophysical properties

The samples were measured in all three directions; the direction parallel to the bedding and lamination is defined as *X*, perpendicular to the lamination as *Y* and perpendicular to the bedding as *Z*. The obtained values of porosity (effective) and density (particle and bulk) are shown in Table 2.

The most porous tuff is the Escolásticas Tuff from Querétaro with 50 % effective porosity; other samples like the GF Black and GF Gray from San Miguel de Allende and the Black QRO from Querétaro have porosities about 40 %. The Chiluca Tuff (CH) with 8 % and the Tenayocátetl Tuff (TY) with 5 % both from Mexico City are the rocks with the lowest porosity (Table 2).

Four samples only show microporosities, (Zac quarry and BP with 97 %, respectively, and BT and LS with 83 %), whereas four samples only show macroporosities, GF black with 96 %, ESC with 94 %, GF gray with 92 % and SMA with 87 %.

Normally it is accepted that the density decreases with increasing porosity, and in the same way it is supposed that by higher porosity less resistance (less cycles) against bursting occurs, but this association cannot be evaluated in the investigated samples (Fig. 1).

Figure 2 shows the relation between the number of cycles in the salt bursting test before the deterioration and the microporosity and Fig. 3 shows the same comparison but with the macroporosity. In the first case (Fig. 2) two groups of samples can be well differentiated. The group with lower values of microporosities deteriorated after a few cycles and the other group clearly shows a trend toward decreasing microporosities, where there is an increase in the number of cycles to deterioration. The other case (Fig. 3) shows the inverse relation.

Table 2 Effective porosity (vol%), particle density (g/cm^3) and bulk density (g/cm^3)

Sample	Porosity (%)	Particle density (g/cm^3)	Bulk density (g/cm^3)
RG red	28	2.60	1.85
SG black	32	2.54	1.73
QRO black	46	2.51	1.35
ZAC quarry	28	2.65	1.90
GF black	49	2.38	1.22
GF gray	45	2.37	1.31
ZAC Cath	32	2.66	1.80
ZAC El Salto	27	2.61	1.90
GR	31	2.55	1.82
BT	18	2.61	2.13
BP	15	2.53	1.84
LS	15	2.34	2.18
CA GDL	41	2.53	1.48
TY	7	2.38	2.26
ESC	50	2.53	1.36
CR	41	2.56	1.53
CH	8	2.58	2.37

The heaviest sample is the Cathedral Tuff from Zacatecas with a density of 2.66 g/cm^3, whereas the Bufa Tuff from Guanajuato was the lightest one with a density of 2.13 g/cm^3.

Comparing the density vs. the number of cycles before deterioration (Fig. 4), we unexpectedly observed a weak tendency that shows that samples with higher density values were less resistant (less cycles) with respect to the lighter samples; however, there are in this case some exceptions.

Pore radii distributions

Pore size distributions were measured using a mercury porosimeter. The pore distributions of all measured tuffs have been put into groups of ideal pore size types, unimodal equal and unequal, and bimodal unequal (Siegesmund and Duerrast 2011).

Four tuffs show an equal unimodal pattern in the micropore zone (TY, BP, ZAC quarry and LS), three tuffs show an equal unimodal pattern in the macropore zone (ESC, GF black and GF gray), five tuffs show a unequal

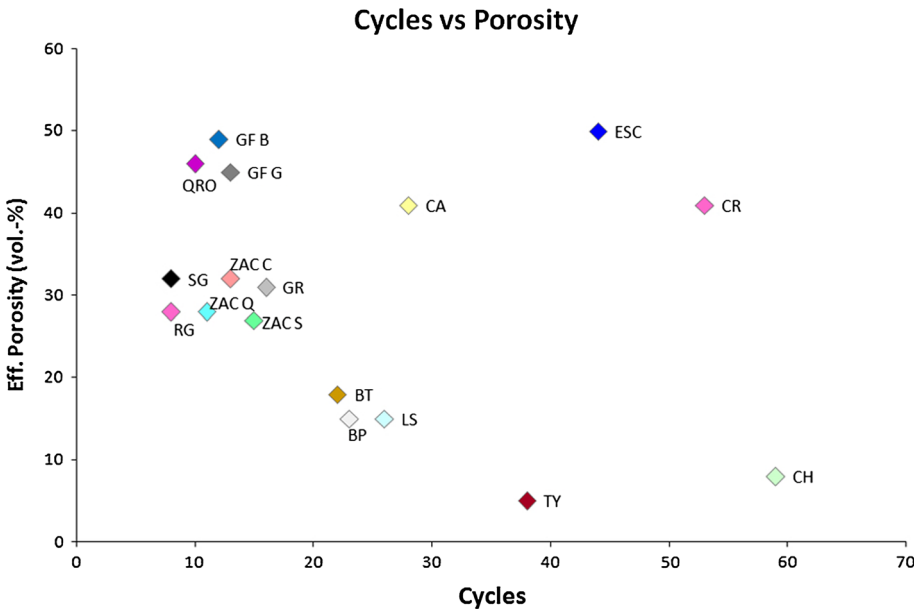

Fig. 1 Correlation of the porosity versus the number of cycles

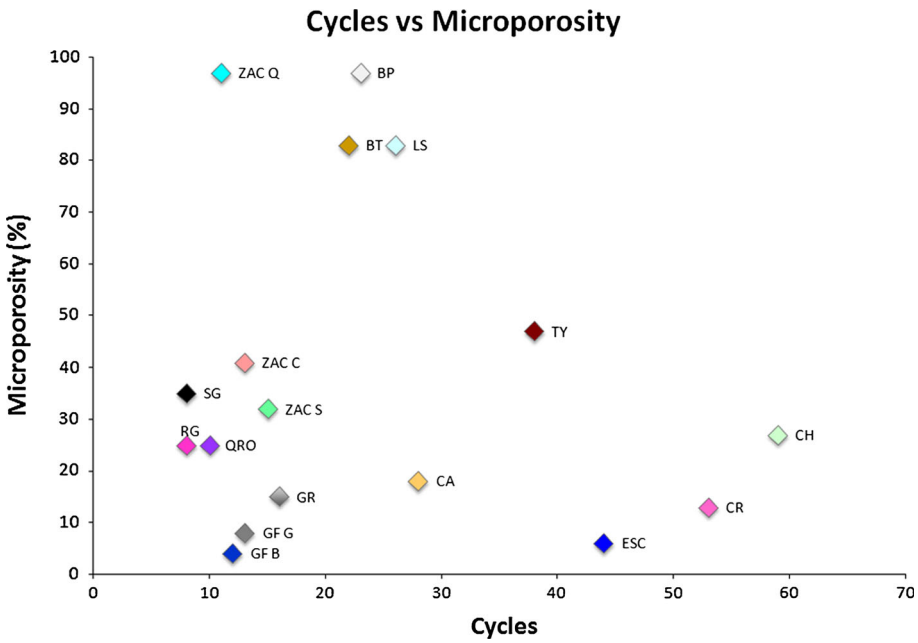

Fig. 2 Correlation of the microporosity versus the number of cycles

bimodal pattern (Qro black, RG red, SG black and GR) and six tuffs are unequal unimodal (BT, CH, CA, Zac El Salto, SMA and ZAC cath).

The most regular pore distribution that shows a normal distribution curve (normal distribution bell) is the CH from Mexico City (Table 3; see also Fig. 12).

Water diffusion

The water vapor diffusion resistance (μ value) provides information about the diffusion resistance of a porous material towards the moisture of the adjacent air (Siegesmund and Duerrast 2011). The values of water diffusion resistance vary between 7.7 (as a minimum, CA Tuff) and 118.5 (as a maximum, CH Tuff). When we plotted the water vapor diffusion resistance vs. the number of cycles of salt bursting (Fig. 5), it is easy to recognize that the CH has the most resistance against the water diffusion. Most of the studied samples have values ranging between 9 and 20.

Water uptake, water absorption

The capillary water absorption of porous materials can be described through the water absorption coefficient

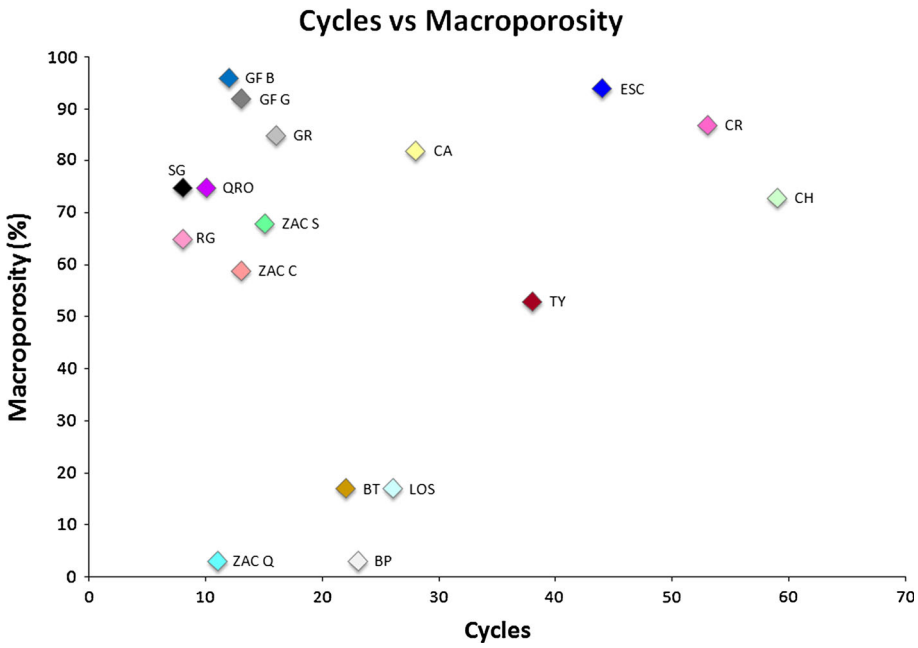

Fig. 3 Correlation of the macroporosity versus the number of cycles

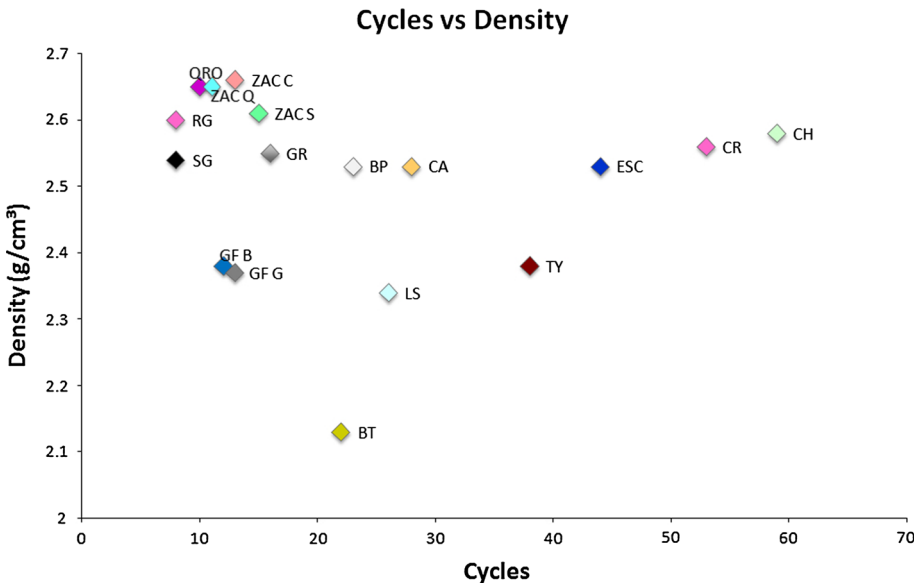

Fig. 4 Correlation of the density versus the number of cycles

(*w* value) and represents the water absorption per unit area vs the square root of the time and initially shows a linear behavior (Siegesmund and Duerrast 2011). Three of the studied samples show almost no absorption with values under 0.5 kg/m$^2\sqrt{}$h (LS 0.04 kg/m$^2\sqrt{}$h; BP 0.14 kg/m$^2\sqrt{}$h and CH 0.4 kg/m$^2\sqrt{}$h). The ESC Tuff shows the highest *w* value with over 30 kg/m$^2\sqrt{}$h. Most of the samples show values ranging between 2 and 10 kg/m$^2\sqrt{}$h. Figure 6 shows that higher porosity corresponds to greater absorption.

If we compare the number of salt bursting cycles versus the obtained *w* values, it is easy to identify different behaviors with respect to the relationship of the *w* value–salt bursting cycles (Fig. 7). There are tuffs with low *w* values but also low number of salt bursting cycles and there is one tuff that has a very low –*w* values, but it is the most resistant against salt crystallization cycles (CH Tuff). This result shows that the water absorption alone does not play the most important role in the decay of tuffs caused by salt crystallization.

Splitting tensile strength

The splitting tensile strength (Brazilian test) was measured under dry and wet conditions in most of the samples. For dry conditions the values vary between 0.9 and 8.2 MPa

Table 3 Pore radii distribution of the analyzed tuffs and percentages of micro- and macropores, porosity and tested cycles

Sample name	Effective pore radii (μm) in porosity (vol%)					% Micropores	% Macropores	Porosity (vol%)	Test-cycles until 30 % material lost
	0.001–0.01 (μm) (%)	0.01–0.1 (μm) (%)	0.1–1 (μm) (%)	1–10 (μm) (%)	10–100 (μm) (%)				
RG red	5	20	11	60	4	25	75	28	8
SG black	11	24	17	43	5	35	65	32	8
Qro black	3	22	14	59	2	25	75	46	10
Zac quarry	4	93	2	1	0	97	3	28	11
GF black	1	3	8	67	21	4	96	49	12
GF gray	2	6	7	77	8	8	92	45	13
Zac Cath	3	38	47	8	3	41	59	32	13
Zac El Salto	5	27	58	8	2	32	68	27	15
GR	0	15	18	55	11	15	85	31	16
BT	4	79	17	0	0	83	17	18	22
BP	7	90	2	1	0	97	3	15	23
LS	21	62	14	2	1	83	17	15	26
CA	3	15	33	47	3	18	82	41	28
TY	9	38	16	20	17	47	53	5	38
ESC	3	3	4	87	3	6	94	50	44
CR	3	10	21	66	1	13	87	41	53
CH	4	23	40	30	3	27	73	8	59

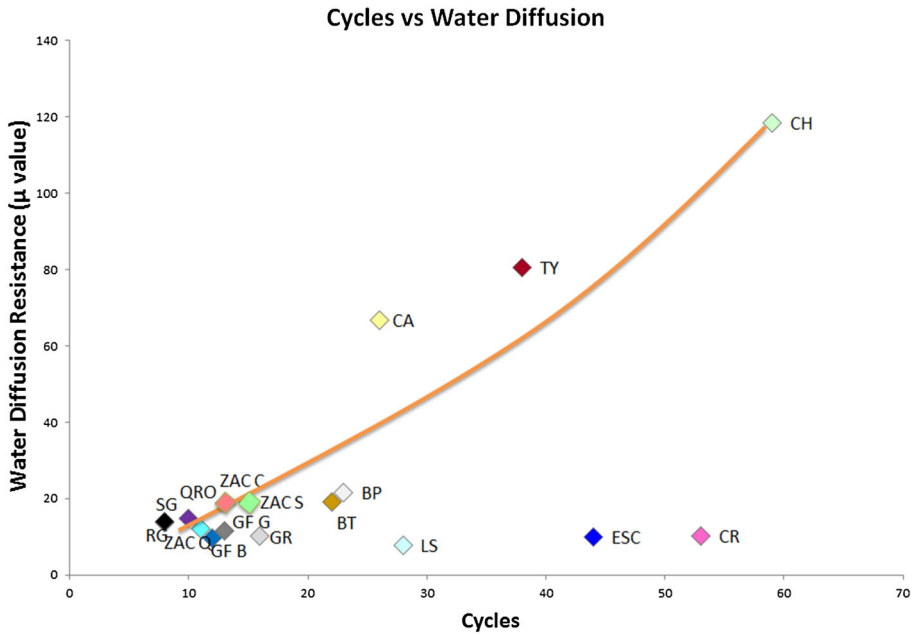

Fig. 5 Correlation of the water vapor diffusion versus the number of cycles

(Table 4) and under wet conditions they vary between 0.49 and 8.71 MPa (Wedekind et al. 2013).

Figure 8 shows a correlation between the percentage of porosity and the tensile strength, and as expected, lower porosity values correspond with higher values of strength. If we compare the strength values with the number of salt bursting cycles (Fig. 9), we can clearly recognize two groups of tuffs. Tuffs with lower values of strength are less resistant against salt bursting and they rapidly deteriorated. The second group with higher strength values shows an inverse trend, so that the strength decreases with an increase in the number of cycles (Fig. 9).

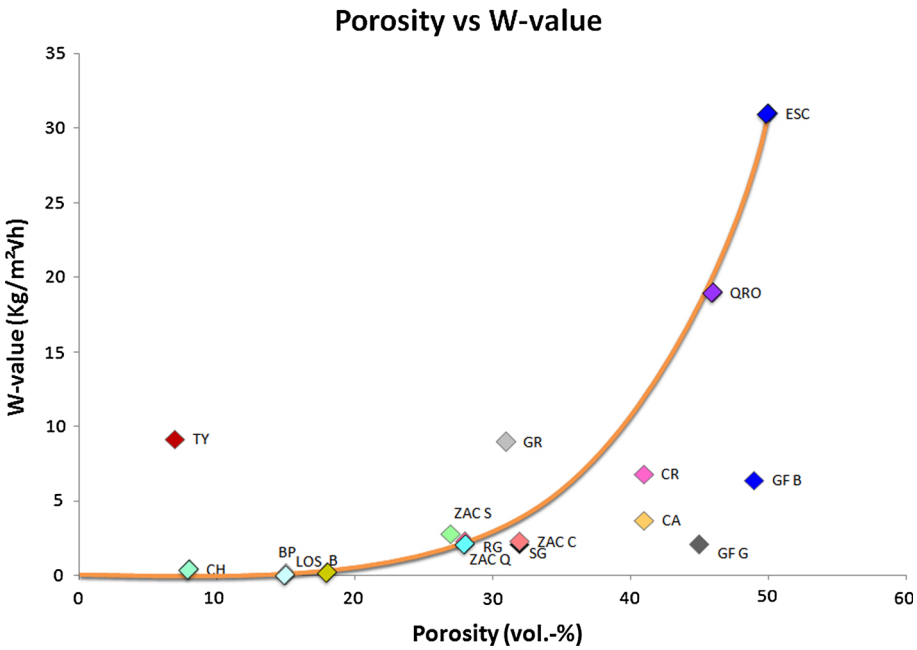

Fig. 6 Correlation of the water uptake versus the porosity

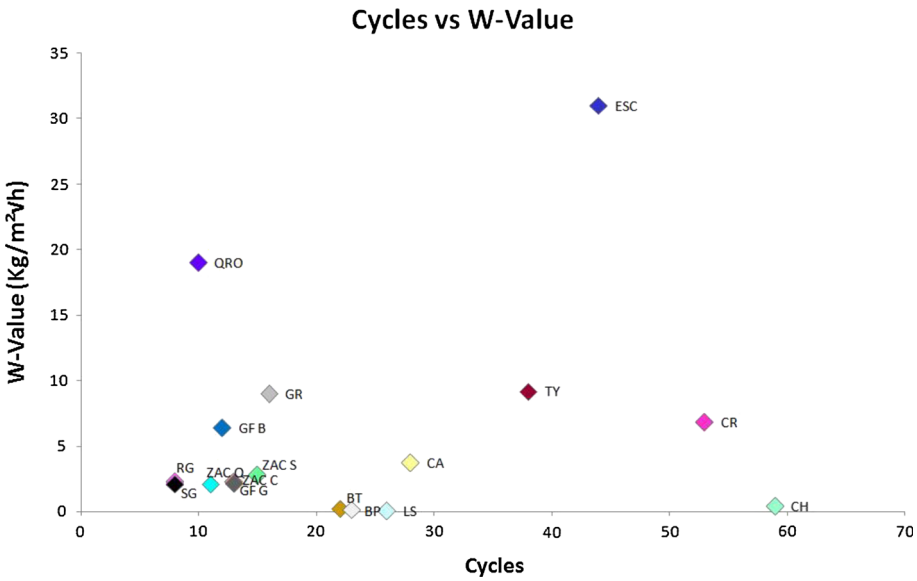

Fig. 7 Correlation of the water uptake versus the number of cycles

Salt weathering tests

It is well known that the common salt weathering test like the European Norm 12370 standard "Natural stone test methods—Determination of resistance to salt crystallization" as well as the RILEM PEM-25 1980, ASTM B 117 or DIN 52 111 test does not seem to be able to reproduce the same weathering conditions as we find in situ. Therefore, new test procedures are under development and discussion (Lubelli et al. 2014).

Salt weathering is a complex process influenced by different parameters like the type or mixture of salts, the climate and humidity conditions and the contamination of the substrate as well as the substrate itself. It seems to be impossible to reproduce all the conditions and possible side effects in the laboratory. Nevertheless, salt weathering tests, performed under laboratory conditions, can give an orientation for determining the salt resistance of porous materials under the performed testing conditions.

Testing procedure

Stone cubes with a dimension of 6.5 cm were used in the testing procedure. The samples were dried until the

Table 4 Splitting tensile strength of the analyzed samples

Sample	Splitting tensile strength dry β_{SZ} (MPa) Maximum	Splitting tensile strength dry β_{SZ} (MPa) Minimum	Anisotropy (%)
RG red	1.6	1.5	6.25
SG black	2.4	0.9	96.25
QRO black	3.0	1.5	50
ZAC quarry	2.4	1.7	29.16
GF black	1.5	1.3	13.33
GF gray	1.9	1.3	31.57
ZAC Cath	3.0	1.5	50
ZAC El Salto	4.2	2.5	40.47
GR[a]	2.2	2.2	0
BT[a]	1.5	1.5	0
BP[a]	6.9	5.8	15.94
LS[a]	8.2	6.2	24.39
CA GDL[a]	1.0	0.9	10
TY[a]	5.7	5.4	5.26
ESC	4.7	2.8	40.42
CR[a]	4.0	3.9	2.5
CH[a]	5.6	5.1	8.92

Anisotropy calculated with $A = n_{max} - n_{min}/n_{max} \times 100$

[a] From Wedekind et al. (2013)

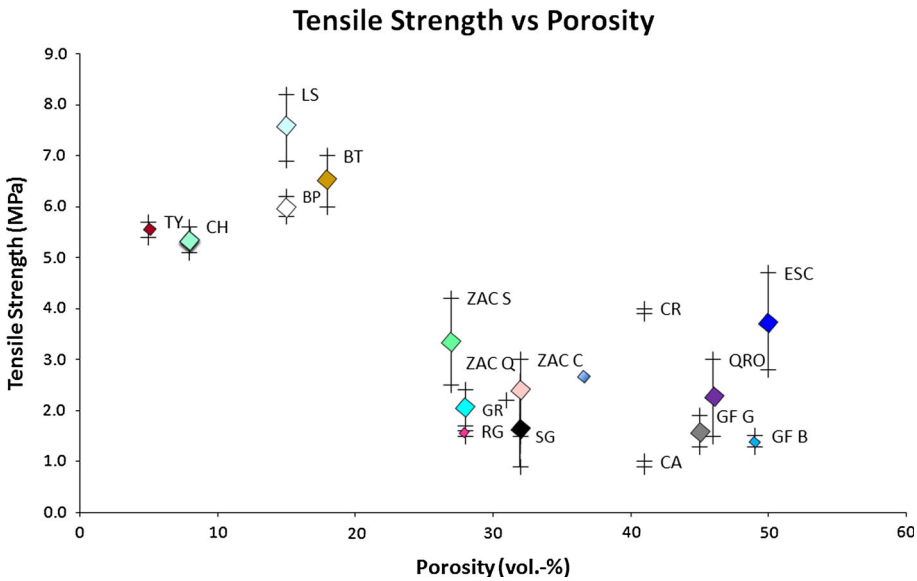

Fig. 8 Correlation of the tensile strength versus the porosity

constant weight was reached and then placed into a closed basket for four hours containing a 10 % solution of sodium sulfate (Na_2SO_4). Afterwards the samples were blotted and put into a heating chamber (60 °C) for at least 24 h. After cooling down to room temperature, the weight change was determined. The procedure was repeated until a mass loss of 30 % could be assumed (Fig. 10).

The salt used for the test is sodium sulfate, which produces a tensile strength up to around 50 MPa depending on the molarity of the supersaturated solution. Therefore, it has the potential to damage nearly all the known natural rocks (Steiger 2005).

The processes that induce stress in the porous material are well investigated in this testing procedure: by drying at

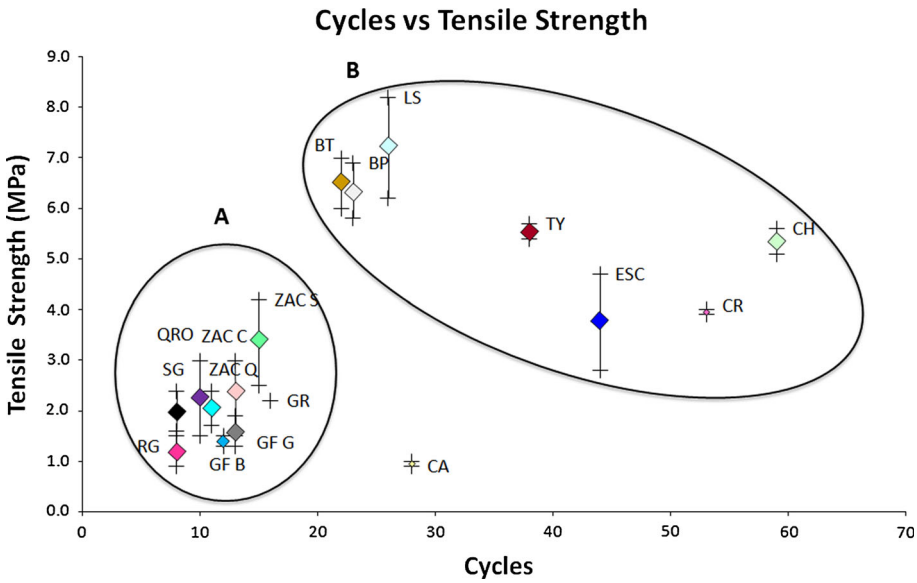

Fig. 9 Correlation of the tensile strength versus the number of cycles

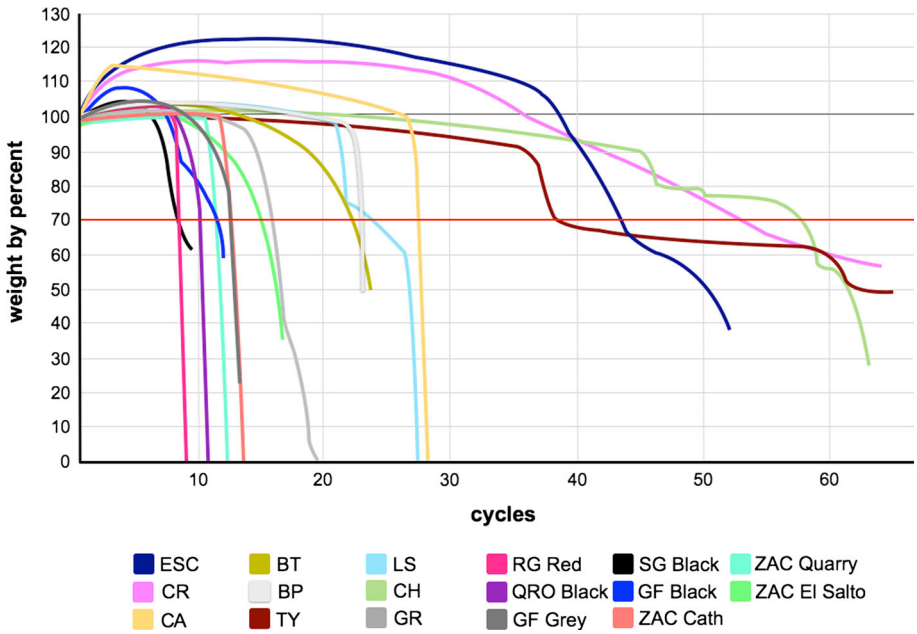

Fig. 10 Correlation of the weight versus the number of testing cycles

60 °C anhydrous Na_2SO_4 crystals are formed while the impregnation leads to their rehydration. The destructive effect is due to the growth of mirabilite crystals precipitated from the highly supersaturated solution originating from the dissolution of anhydrous Na_2SO_4 during re-wetting (Flatt 2002).

General observations of the salt weathering test

During the first testing cycles most of the samples show an increase in weight, due to storage of salt within the porous structure. For some samples even an increase in weight could be assumed, while at the same time an observable material loss took place. Other samples show a nearly constant weight during the first cycles and after a continuous material loss (Fig. 10).

Observations of destruction during the salt bursting test and the deterioration forms in the field are described below, starting with the lower to the higher salt bursting resistance:

- RG from San Miguel de Allende
  RG shows a plane flaking of the matrix as well as a rounding of the edges and upper corners. After five cycles initial destruction begins in the sample by the

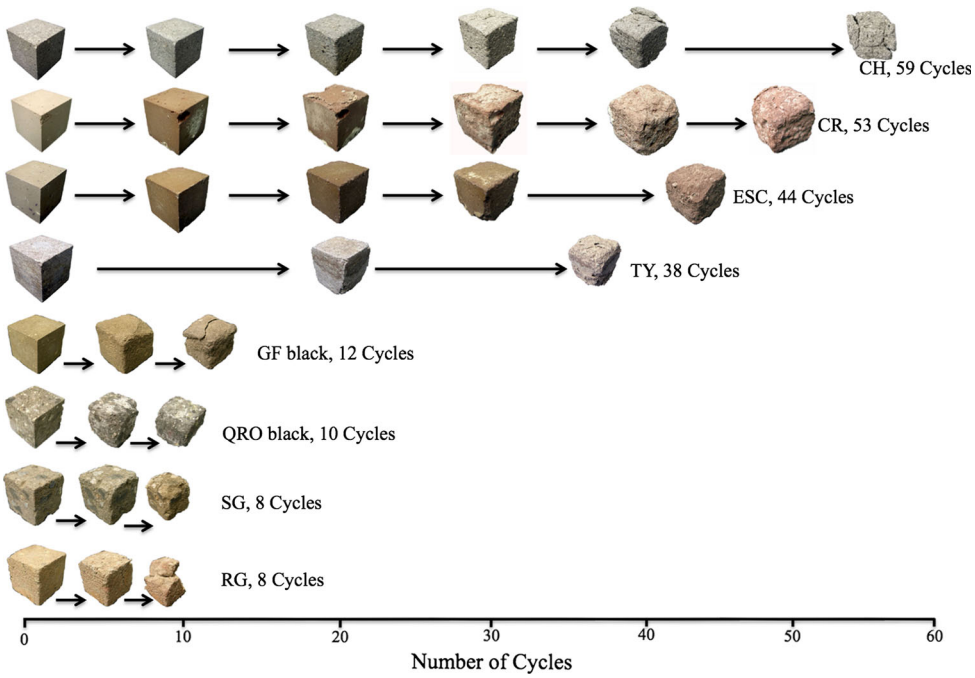

Fig. 11 Photographic documentation of the salt bursting test of the four most resistant and the four less resistant investigated tuffs (also compare with Fig. 12)

development of structural cracks. The vulnerability to salt weathering can be observed at several buildings, for example, at the windows and door frames in the city of San Miguel de Allende (Plate 1b; Fig. 11).

- SG from San Miguel de Allende
  During the salt bursting test a weathering out of the basaltic inclusions takes place as well as a flaking of the matrix, comparable to RG. If the stone is contaminated with salt, the same weathering forms can be observed in the field (Plate 1a; Fig. 11).
- Qro black from Querétaro
  The black tuff from Querétaro shows a loss of both components and matrix after the salt bursting test. Deterioration can be characterized by disjointing and scaling of weak components, like clasts and the disintegration (e.g., dissolution) of the matrix. Nearly the same weathering phenomena can be observed in the field (Fig. 11).
- Zac quarry from Zacatecas
  The sample from the Guadalupe quarry shows a plane flaking of the matrix as well as a rounding of the edges and loss of corners. After nine cycles the sample lost more than 80 % of its material (Plate 1e).
- GF Black and GF gray from San Miguel de Allende
  Both tuffs show a similar development in the salt bursting test. At the beginning both samples show an increase in their volume of about 10 %, but after the 7th cycle the decay begins mainly at the edges. After the 10th cycle in the GF gray, a very rapid back-weathering occurs mainly parallel to the lamination (*X*–*Y* plane). GF black lost material mostly at the edges and not in the laminations. GF gray lost more than 30 % of its material after 12 cycles and GF black 30 % after 13 cycles (Fig. 11).
- Zac Cath. from Zacatecas
  The sample from the cathedral shows a loss of grains (sugaring) and flaking of the matrix. After 12 cycles the sample was completely useless and destroyed.
- Zac El Salto from Zacatecas
  The sample from El Salto shows a loss of only single grains, possibly due to its weak mineral components such as feldspar. After 13 cycles the sample had lost a significant amount of material.
- GR from Mexico City
  After four cycles a rounding at the upper edges starts by the flaking of the matrix as well as in the inclusions. After 10 cycles the sample shows a nearly round form. Only the inner flat areas remain nearly undamaged by forming a crust. In the field the same weathering phenomena can be observed.
- BT from Guanajuato
  The deterioration of the Bufa Tuff starts by the back-weathering of soft bound whitish inclusions. After eight cycles the first cracks are breaking away at the corners. The matrix is starting to flake from the upper edges during the following cycles. After 12 cycles cracks form parallel to the flow or bedding structure of the stone.
- BP from Hidalgo
  After eight cycles first low bound particles are weathered out at the edges and the bottom of the sample cube. In the 14th cycle the upper edges start to split.

Furthermore, the sample breaks and cracks are created parallel to the bedding. This weathering form can also be observed in the field, like for example at several buildings in Mexico City.

- LS from Guanajuato
  The deterioration of the Loseros Tuff starts by the weathering of defined layers after 10 cycles. At the same time a crust also forms that breaks away parallel to the surface but perpendicular to the bedding. This weathering form can be observed at several buildings in Guanajuato as well as in Guadalajara where the stone was used for tomb monuments (Plate 1d).
- CA from Jalisco
  The lost of material starts within the yellow pumice inclusions. They weather out after the second cycle. A tendency of rounding also takes place. After total saturation by salt within the highly porous structure the stone starts to break after the 20th cycle, which leads to total destruction.
- TY Tenayocátetl from Mexico City
  The stone shows two different stages of weathering. After the 14th cycle some grains are lost at the edges. Comparable to the Loseros Tuff, the Tenayacétetl Tuff first develops a crust on the surface of the material even perpendicular to the bedding. After this, the crust splits away in scales and by the 35th cycle a rounding by flaking takes place. Both weathering forms can be found in the field, e.g., at the Templo Mayor in Mexico City (Fig. 11).
- ESC from Querétaro
  The tuff of Queretaro shows an increase of weight of around 20 % in the first 40 cycles by storing salt within the highly porous structure. First damages can be recognized after the 15th cycle by a slight rounding at the edges. After the 30th cycle the corners at the bottom start to weather back. A significant loss of material takes place after the 40th cycle by the breaking out of small rock fragments (Plate 1f; Fig. 11).
- CR from San Miguel El Alto
  Comparable with the Cantera Amarilla de Guadalajara, the weathering of the Red Tuff from San Miguel del Alto starts by the weathering of the pumice inclusions. A damage of the shape starts quite late. After about the 30th cycle a rounding by flaking starts in the smaller particles. Similar weathering forms can be found in the field (Fig. 11).
- CH from Mexico City
  The deterioration of the CH starts with a rounding of the edges after the 15th cycle. Later on, after the 45th cycle a splitting of a crust with a thickness of around 1.5 cm occurs. This starts at the upper area of the sample and leads to a stepwise reduction and rounding. Similar weathering forms can be observed on site at the cathedral and in several other palaces in Mexico City (Fig. 11).

Discussion

Characterization of the pore space

The damage potential of salt crystallization depends on the pore size distribution as well as on the type of pore radii distribution. A unimodal distribution containing only micropores is particularly susceptible to salt weathering (Snethlage 1984; Scherer 1999; Ruedrich and Siegesmund 2007). Crystallization pressures can only occur in pores with pore radii smaller than 30 nm (Rijniers et al. 2005) ore 50 nm (Steiger et al. 2011; Siegesmund and Steiger 2007). The most dangerous pore dimensions for salt crystallization are the pores that range around 1 μm (Benavante 2011). These critical pores are developed as a secondary porosity by the storage of salt during accumulation (Angeli et al. 2008).

Tuff rocks with only micropores, e.g., TY, BP and Zac quarry show a highly variable response to the salt bursting test resisting 38, 23 and 11 cycles, respectively, before the destruction. Samples with practically only macropores, e.g., ESC, GF black and GF gray, showed a similar behavior with 44, 12 and 13 cycles before complete decay (Fig. 12).

Our investigations, however, clearly show that the tuffs with less cycles endurance have high porosity values (ranging between 28 and 49 %). All of the tuffs show a well developed bimodal pore radii distribution, with an important percentage of microporosity but also higher values of macroporosity (Fig. 13).

Characterization of the physical and moisture properties

No clear correlation can be observed when comparing the weight reduction by salt bursting test cycles with the splitting tensile strength of the investigated samples (Fig. 9). Nevertheless, two possible tendencies are discernible in Fig. 9 and these are shown as groups labeled areas (a) and (b). Group a: the vulcanites show a low resistance against salt weathering related to the strength of the material as measured by the splitting tensile strength test. The clearly defined group of samples at the bottom part of the marked area contains most of the investigated samples, i.e., SG Black and RG Red, QRO Black, ZAC Quarry, GF Black, ZAC Cath, GF Gray, ZAC El Salto and CA and GR. Most of these samples are dominated by a macroporous structure. Only the sample ZAC Quarry with 97 % is clearly dominated by micropores. The other

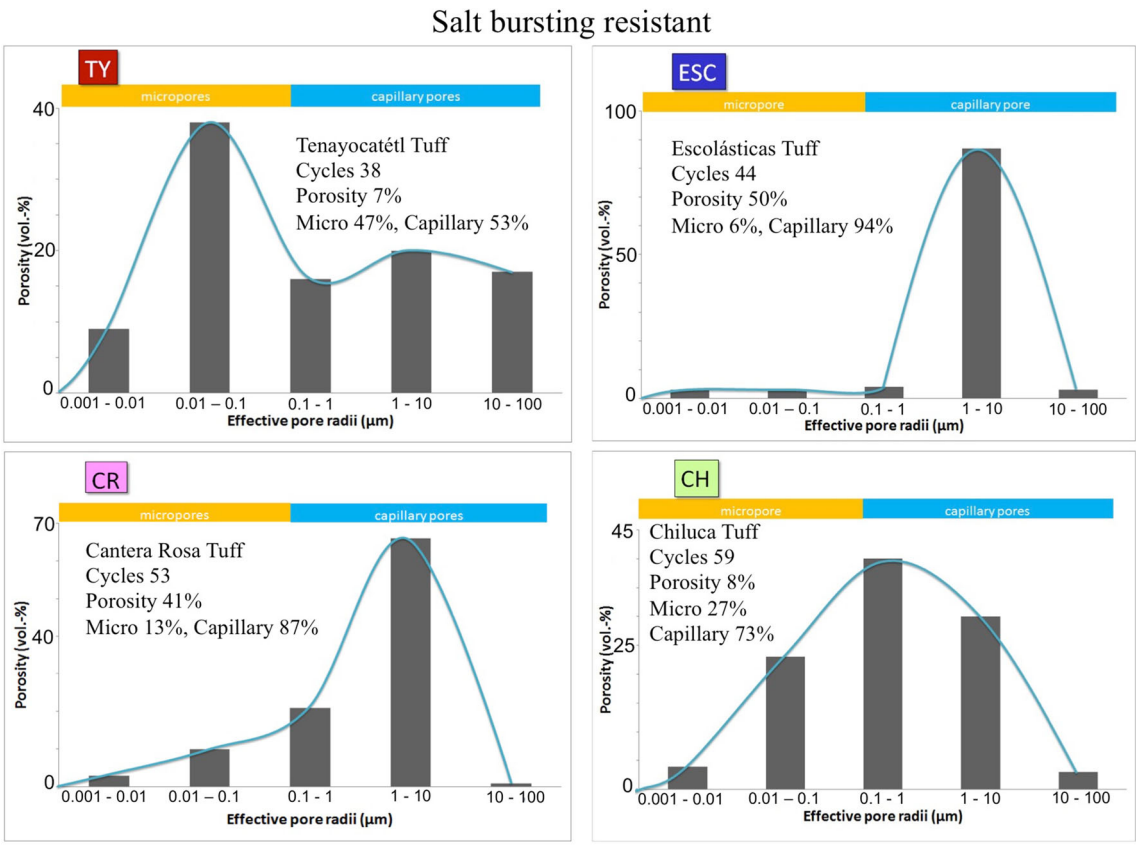

Fig. 12 Comparison of the different pore radii distributions of the four most resistant tuffs against salt bursting

samples have an averaged amount of microporosity containing only 18 %. However, all the samples can be defined as low bound stones with low mechanical values as defined by the splitting tensile strength values between 1.4 and 3 MPa (see Fig. 8).

The three samples in the upper part of area a, BT, BP and LS are characterized by a comparably higher mechanical strength, but they are clearly dominated by microporosity, with an average of 88 %. This significant amount of micropores is probably the reason they are resistant against salt crystallization, a similar tendency has been noted with investigated sandstones by different researchers (Benavante 2011; Ruedrich and Siegesmund 2007).

Group b: The TY, ESC, CA and CH are characterized by a comparable relation of micropores and macropores. In the case of TY this relation is nearly balanced. The CH-Tuff with the highest salt resistance of all investigated tuffs contains a microporosity of 27 % and a macroporosity of 73 % (Fig. 12).

Some important aspects appear to play a decisive role because the CH Tuff is the most resistant rock against salt bursting.

1. CH together with TY is the less porous of the studied tuffs with 8 and 7 % porosity, respectively.
2. CH is dominated by the presence of macroporosity (73 % macropores); however, it is the tuff that shows the most balanced pore radii distribution, forming an almost ideal distribution curve (Fig. 12).
3. Two moisture properties appear to be critical in the high resistance to salt crystallization of the CH Tuff. (1) The extremely poor ability to absorb water (water uptake) which is 0.4 (Fig. 7), and (2) CH has the highest resistance to water diffusion with 118.5 (Fig. 5), i.e., CH is a rock that shows little absorption and hardly allows the diffusion. These two features together with the low porosity and its balanced pore distribution are the factors that differentiate it from the other tuffs.

The significant salt resistance of the other three tuff rocks in this group seems to be related to the porous network as well as to mineralogical aspects. It becomes clear, that during the first testing cycles an increase of weight reaching up to 25 % (ESC, CR and CA) takes place (Fig. 10). This increase can be related to the high porosity of the samples containing 41 % (CA, CR) and 50 % (ESC). The increases in weight can be due to the storage of salt, but also due to the water retention of the material. This water retention is not related to a poorly connected pore

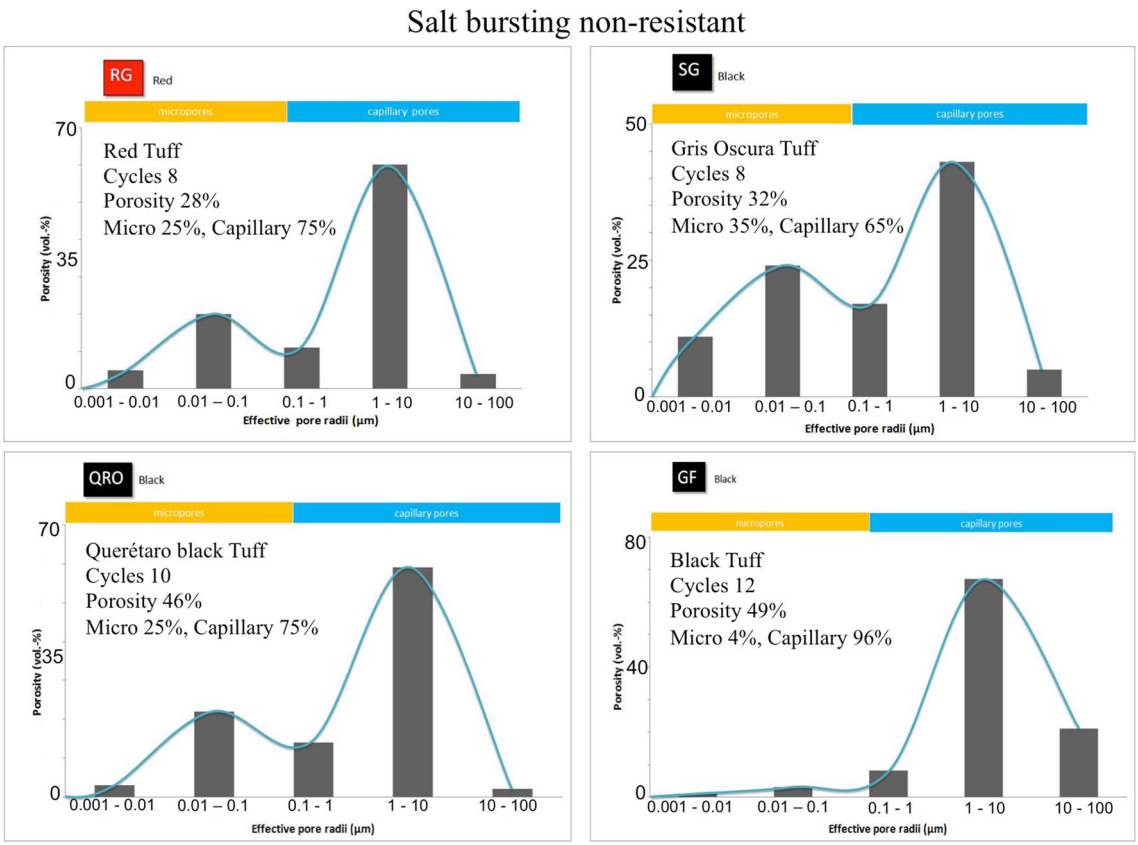

Fig. 13 Comparison of the different pore radii distributions of the four less resistant tuffs against salt bursting

percentage. These three tuffs have a quite low water vapor diffusion capacity of 7.7 (CA), 9.9 (ESC) and 10.3 (CR) and does not contain a high amount of swellable clay minerals (Wedekind et al. 2012).

An explanation for this could be fine mineralogical structures in these samples visible by SEM (Plate 5). The ESC Tuff, for example shows quartz (cristobalite) crystals, grains and little pumice clasts that are embedded in a very fine-grained matrix, which has a microporous fibrous texture similar to zeolites (Plate 5a, b). A well-known property of zeolite minerals is a high water retention capacity used widely for soil fertilization (De Campos Bernardi et al. 2010; Torkashvand and Shadparvar 2013) and this property is related to their complicated microstructure. In the case of the CA Tuff amicite and also kaolinite minerals are clearly identifiable by the SEM, and these could play a role in water retention (Plate 5c). The porous texture of the CA Tuff as well as the SMA Tuff is covered by a fine fibrous structure. In the case of the CA Tuff EDX analyses show Na^+ and K^+-rich components, probably amicite minerals that belong to the amicite-phillipsite zeolite series (Plate 5d). Closer investigations to the question if zeolites are present in the investigated samples show that in the BP-Tuff zeolites could also be found. Nevertheless, the presence of zeolite minerals does not seem to play a significant role in the resistance against salt weathering in the investigated tuff rocks. After 23 cycles a nearly total destruction of the BT-Tuff took place (Table 3; Fig. 11). Almost everywhere in the matrix of the SMA-Tuff fine magnetite structures could be identified (Plate 5e) as well as Mn–Ba-rich mineralizations, probably hausmannite and psilomelane associated with a fine needle-like structure (Plate 5f).

The RG and SG Tuffs, which are less resistant to salt crystallization (both can only withstand 8 cycles) show a very well interconnected open porous network (Plate 6a, c). They exhibit remarkable weathering patterns, both in the matrix and in the clasts (Plate 6b, d), clearly causing a primary and a secondary porosity that allows the rapid formation of salt crystals inside the tuff (see Figs. 10, 11).

Conclusions

The results of our investigations conclude some special aspects regarding the resistance of the volcanic tuff rocks against the salt bursting. Some of our results can be confirmed for similar tests on different rocks.

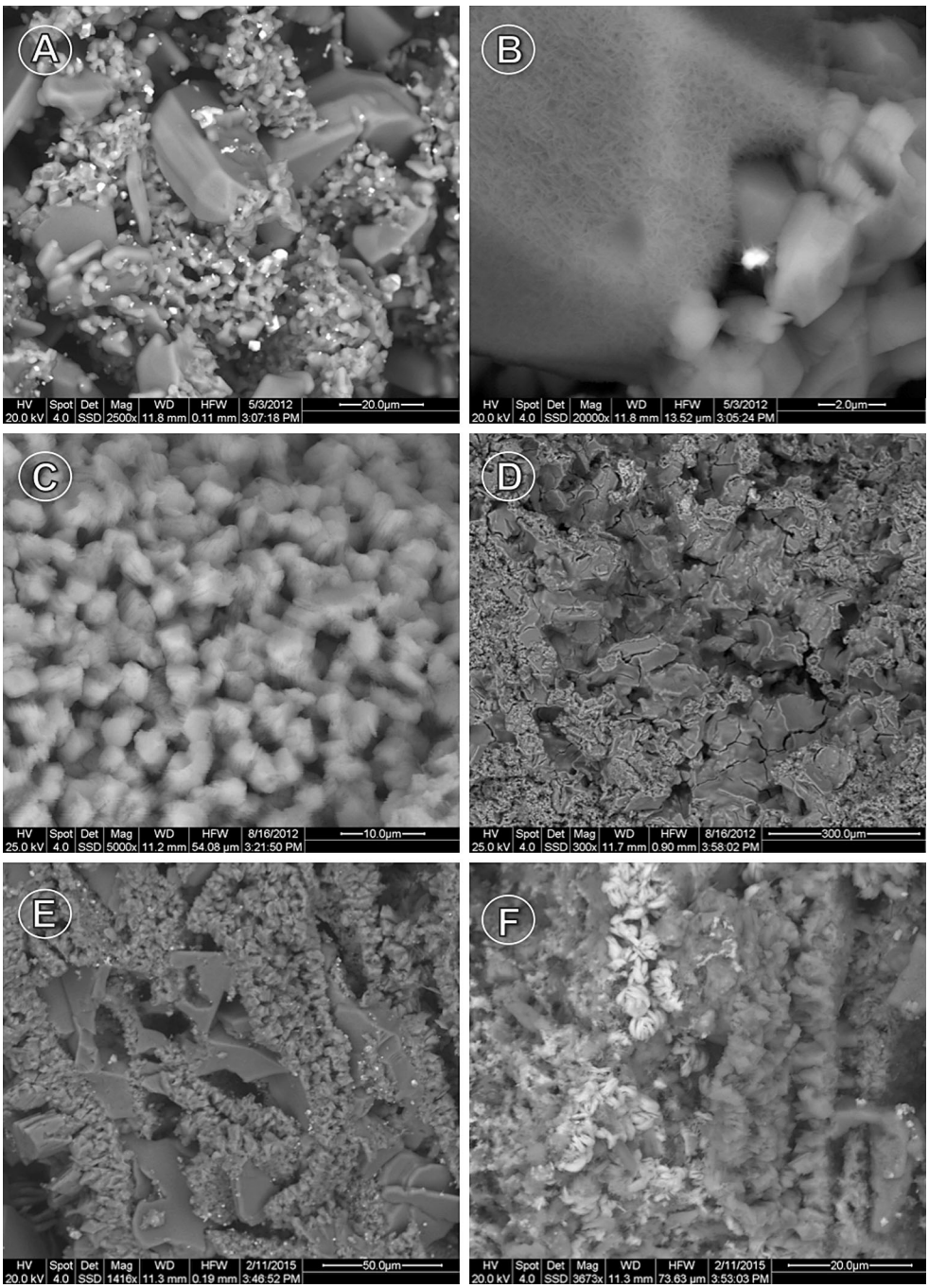

Plate 5 Scanning electron microscopy (SEM) images of the ESC, CA and CR Tuffs. **a** Cristobalite crystals overlayered by a fibrous mineralogical structure within the pore space of ESC. **b** The fine fibrous structure in detail. **c** Kaolinite and amicite crystals forming a complex pore network in the matrix of the CA Tuff. **d** Amicite-phillipsite zeolite and probably kaolinite produced by the alteration of feldspar and located within larger pores of the same sample. **e** Quartz in the center surrounded by very fine-grained K-feldspar. **f** Mn–Ba mineralization (probably hausmannite/psilomelane) in the CR Tuff, together with fine-grained chlorite needles

Our results show that the resistance to the salt bursting decreases with the increase in porosity. The rocks with higher porosity resisted less to cycles of salt crystallization. In fact the two studied samples with the lowest porosities resist the majority salt bursting cycles (TY and CH, Figs. 10, 11, 12). However, the rock with the highest porosity (ESC with 50 % porosity) was extremely resistant to salt crystallization, indicating that the porosity itself is not the determining factor in this resistance.

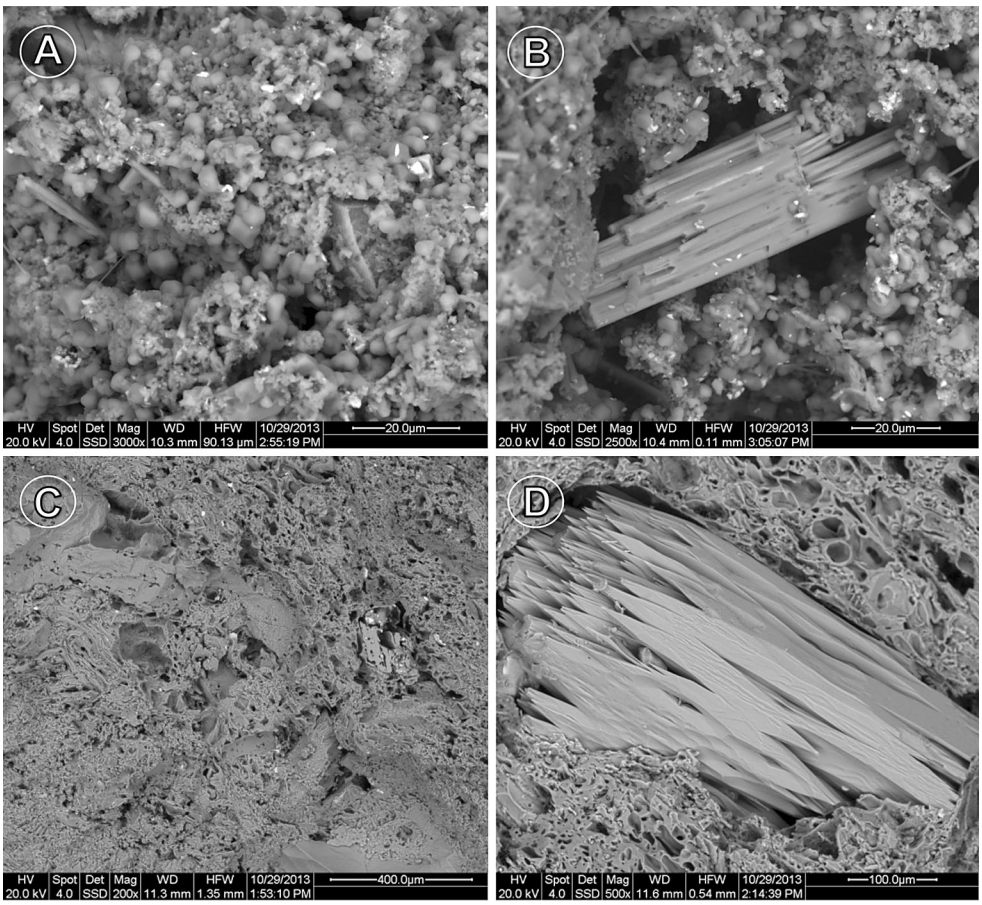

Plate 6 Scanning electron microscopy (SEM) images of the RG and SG tuffs. **a** Overview of the RG tuff with abundant SiO_2 particles. The porous matrix is clearly visible in this tuff. **b** Clast with observable weathering marks, which creates a secondary porosity. **c** Overview of the SG tuff, which is similar to RG with its prominent very porous glassy matrix. **d** Probable pumice clast, strongly weathered and embedded in a glassy matrix of the SG tuff

Another factor that can influence the resistance against salt crystallization is the capacity of water uptake. Salts are dissolved in the absorbed water so that it is expected that rocks with higher water uptake values should have more possibilities for allowing salt crystallization to occur. Four of the most resistant tuff rocks showed very low values of water uptake (w value around zero, Fig. 7). The samples with the lowest resistance did not show any important w values (around 2–5).

Finally, two factors appear to have a real importance concerning the resistance against salt crystallization, the water vapor diffusion (μ value) and the pore radii distribution. This study clearly shows that the CH tuff rock had the highest vapor diffusion resistance value and its pore radii distribution was the only one with a well-distributed spectrum (Fig. 12). On the other hand, the less resistant tuff rocks almost invariably show an unequal bimodal pore distribution pattern and have vapor diffusion values between 5 and 10 (Fig. 12).

The results also show that salt resistance is not only controlled by the porous structure, but also by the mechanical strength. A fast and mostly total destruction takes place, if the stone only reaches a splitting tensile strength up to 3 MPa (Fig. 9). This value of low mechanical strength can be defined as a critical value in regard to salt weathering. Furthermore, in the case of a very low mechanical strength the pore size distribution seems to play a minor role.

Clearly, microporosity becomes a relevant factor for rapid salt destruction if it reaches more than 50 % of the pore volume (Figs. 12, 13). If the matrix of the tuff contains a high amount of the described micro-mineral structures and textures, the salt resistance can increase in a significant way even if the material only reaches a low splitting tensile strength. This can be seen in the ESC-, the CA-, and the SMA-Tuff (probably including glass and zeolites minerals).

The tuff rocks that show a lesser resistance to salt crystallization lose more than a third of their weight by barely

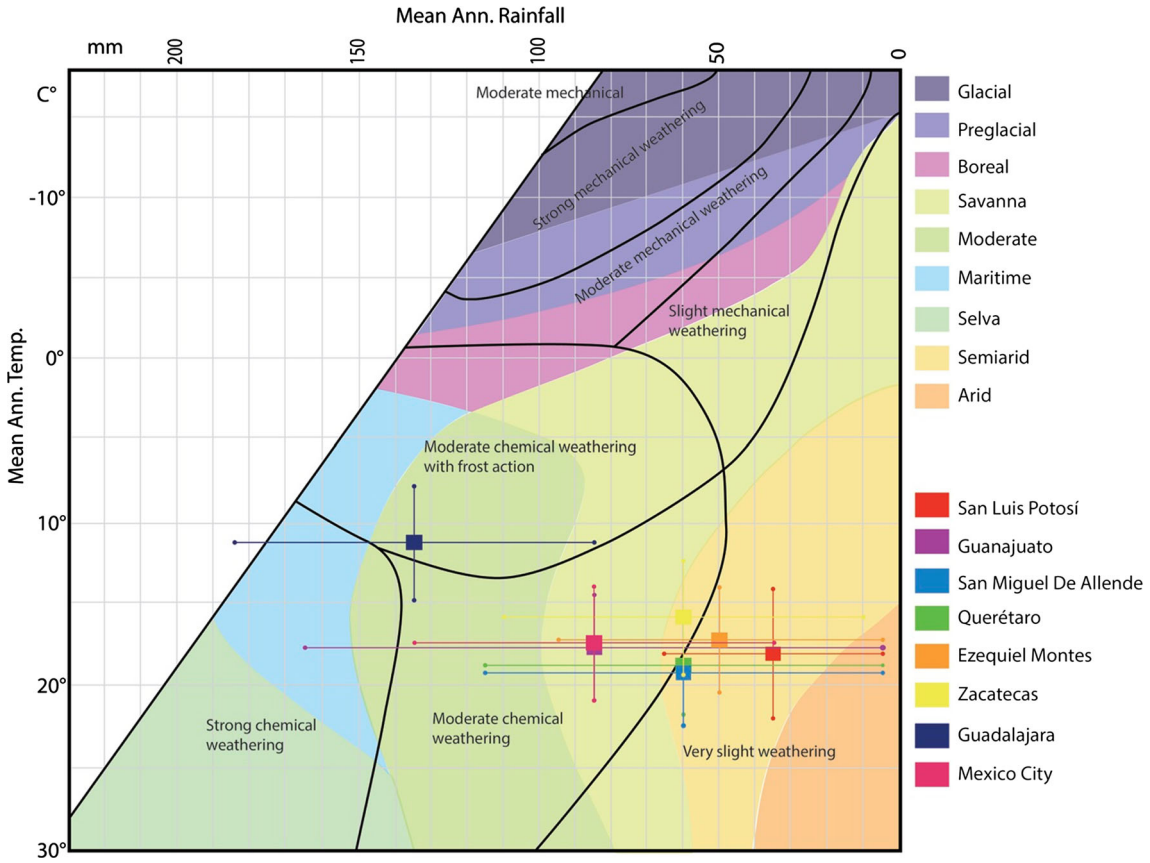

Fig. 14 Location of the principal cities, where the analyzed samples were taken with respect to the "morphogenic regions" of Peltier (1950) and the "types of weathering" of Fookes et al. (1971)

being able to withstand 8 cycles, therefore it is to be expected that the damages in the old historical buildings constructed with these rocks should be notable. However, the damages are indeed locally very strong, but the constructions, some of them more than 200 years old are still standing and many of them are in good condition and without the expected damage. We have noticed that the porosity, its diameter and pore size and its moisture properties such as the water uptake and vapor diffusion together with the mineralogical properties and fabrics of the rock play major roles in the ability of a rock to allow or prevent salt crystallization. The main element for the transport of salts is water. Water in any form is the main factor for the transport of solvents and the crystallization of salt. When there is no water, no crystallization occurs. This factor explains the relatively little damage to buildings erected with these so erodible rocks. Plotting the meteorological data from the cities and regions where the analyzed samples are used as construction materials into the combined rainfall/temperature diagram of Peltier (1950) and Fookes et al. (1971) (Fig. 14), it is easy to see that the tuff rocks of San Miguel de Allende and Querétaro, both less resistant to salt bursting, fall into the semiarid region and in the area with very slight weathering (Fig. 14). This may be the reason why these weak and soft rocks show such a good resistance against weathering and why they are still being used as natural building stone in Mexico today.

Acknowledgments Our work was supported by the Consejo Nacional de Ciencia y Tecnología, (CONACyT), Projects Ciencia Básica (CB-130282) and Cooperación Bilateral (191044), the German Science Foundation (DFG Si-438/44-1) and the Hans-Boeckler-Foundation. We are grateful to Erasmo Mata, Alejandro Rivera, Theresa Platz, Christopher Pötzl, Eneida Molina, Detlev Klosa, M. Sitnikova and Nohemi Cardona for their technical and laboratory support. Finally, the authors would also like to thank the two anonymous reviewers who with their thoughtful suggestions substantially improved this manuscript.

References

Angeli M, Bigas JP, Benavente D, Menéndez B, Hébert R, David C (2007) Salt crystallization in pores: quantification and estimation of damage. Environ Geol 52:205–214

Angeli M, Benavente D, Bigas JP, Menéndez B, Hébert R, David CH (2008) Modification of the porous network by salt crystallization in experimentally weathered sedimentary stones. Mater Struct 41:1091–1108

Benavante D (2011) Why pore size is important in the deterioration of porous stones used in the build heritage. Macla, no. 15, Revista de la Sociedad Española de Mineralogia, Barcelona, p 41–42

Coussy O (2006) Deformation and stress from in-pore drying-induced crystallization of salt. J Mech Phys Solid 54(8):1517–1547

De Campos Bernardi AC, Peronti Anchão Oliviera P, De Melo Monte MB, Polidoro JC, Souza-Barros F (2010) Brazilian sedimentary zeolite use in agriculture. In: 19th world congress of soil science, soil solutions for a changing world 1–6 August 2010, Brisbane, Australia

Fitzner B, Snethlage R (1982) Einfluß der Porenradienverteilung auf das Verwitterungsverhalten asugewälter Sandsteine. Bautenschutz Bausanierung 5(3):97–103

Flatt RJ (2002) Salt damage in porous materials: how high supersaturations are generated. J Cryst Growth 242:435–454

Fookes PG, Dearman WR, Franklin JA (1971) Some engineering aspects of rock weathering with field examples from Dartmoor and elsewhere. Q J Eng GeolHydrogeol 4:139–185. doi:10.1144/GSL.QJEG.004.03.01

Grossi CM, Esbert RM (1994) Las sales solubles en el deterioro de rocas monumentales: revisión bibliográfica. Mater Construc 44(235):15–30

Lubelli B, van Hees RPJ, Nijland TG (2014) Salt crystallization damage: how realistic are existing ageing tests? In: De Clercq H (ed) SWBSS 2014 3th International Conference on Salt Weathering of Buildings and Stone Sculptures, Brussels, 14–16 October 2014, Royal Institute for Cultural Heritage (KIK/IRPA), pp 259–274

Peltier L (1950) The geographic cycle in periglacial regions as it is related to climatic geomorphology. Ann Assoc Am Geol 40:214–236

Rijniers LA, Huinink HP, Pel L, Kopinga K (2005) Experimental evidence of crystallization pressure inside porous media. Phys Rev Lett 94(7):075503-1–075503-4

Rodriguez-Navarro C, Doehne E (1999) Salt weathering: influence of evaporation rate, supersaturation and crystallization pattern. Earth Surf Proc Land 24:191–209

Ruedrich J, Siegesmund S (2006) Fabric dependence of length change behaviour induced by ice crystallisation in the pore space of natural building stones. In: Fort R, Alvarez de Buergo M, Gomez-Heras M (eds) Heritage, weathering and conservation. Taylor & Francis, London, pp 497–505

Ruedrich J, Siegesmund S (2007) Salt and ice crystallization in porous sandstones. Environ Geol 52:225–249

Scherer GW (1999) Crystallization in pores. Cem Concr Res 29:1347–1358

Siegesmund S, Duerrast H (2011) Physical and mechanical properties of rocks. In: Siegesmund S, Snethlage R (eds) Stone in architecture: properties, durability, 4th edn. Springer, Berlin, pp 97–225

Siegesmund S, Steiger M (2007) Special issue on salt decay. Environ Geol 52:185–420

Snethlage R (1984) Steinkonservierung. Arbeitsheft Bayer. Landesamt f. Denkmalpflege, 22, Munich

Steiger M (2005) Crystal growth in porous materials—I: the crystallization pressure of large crystals. J Cryst Growth 282:455–469

Steiger M, Carola AE, Sterflinger K (2011) (2013) Chapter 4—weathering and deterioration. In: Siegesmund S, Snethlage R (eds) Stone in architecture. Springer, Berlin/New York, pp 227–316

Torkashvand AM, Shadparvar V (2013) Effect of some organic waste and zeolite on water holding capacity and PWP delay of soil. Curr Biotica 6(4):459–465

Tsui N, Flatt RJ, Scherer GW (2003) Crystallization damage by sodium sulphate. J Cult Herit 4:109–115

Wedekind W, Ruedrich J, Siegesmund S (2011) Natural building stones of Mexico–Tenochtitlán: their use, weathering and rock properties at the Templo Mayor, Palace Heras Soto and the Metropolitan Cathedral. Environ Earth Sci 63(7/8):1787–1798

Wedekind W, López-Doncel R, Dohrmann R and Siegesmund S (2012) Hygric and hydric expansion of tuffs exclusively caused by clay minerals?—12th International Conference on the deterioriation and conservation of Stones, Extend abstracts book, New York (in press)

Wedekind W, López-Doncel R, Dohrmann R, Kocher M, Siegesmund S (2013) Weathering and deterioration of volcanic tuff rocks used as building stone causes by moisture expansion. Environ Earth Sci 69:1203–1224. doi:10.1007/s12665-012-2158-1

Winkler EM, Singer PC (1972) Crystallization pressure of salts in stone and concrete. Geol Soc Am Bull 83:3509–3514